

Universality of the Collins-Soper kernel in lattice calculations

Hai-Tao Shu,¹ Maximilian Schlemmer,¹ Tobias Sizmann,¹ Alexey Vladimirov,²
Lisa Walter,¹ Michael Engelhardt,³ Andreas Schäfer,¹ and Yi-Bo Yang^{4, 5, 6, 7}

¹*Institut für Theoretische Physik, Universität Regensburg, D-93040 Regensburg, Germany*

²*Departamento de Física Teórica & IPARCOS, Universidad Complutense de Madrid, E-28040 Madrid, Spain*

³*Department of Physics, New Mexico State University, Las Cruces, NM 88003, USA*

⁴*CAS Key Laboratory of Theoretical Physics, Institute of Theoretical Physics,
Chinese Academy of Sciences, Beijing 100190, China*

⁵*School of Fundamental Physics and Mathematical Sciences,
Hangzhou Institute for Advanced Study, UCAS, Hangzhou 310024, China*

⁶*International Centre for Theoretical Physics Asia-Pacific, Beijing/Hangzhou, China*

⁷*School of Physical Sciences, University of Chinese Academy of Sciences, Beijing 100049, China*

The Collins-Soper (CS) kernel is a nonperturbative function that characterizes the rapidity evolution of transverse-momentum-dependent parton distribution functions (TMDPDFs) and wave functions. In this Letter, we calculate the CS kernel for pion and proton targets and for quasi-TMDPDFs of leading and next-to-leading power. The calculations are carried out on the CLS ensemble H101 with dynamical $N_f = 2 + 1$ clover-improved Wilson fermions. Our analyses demonstrate the consistency of different lattice extractions of the CS kernel for mesons and baryons, as well as for twist-two and twist-three operators, even though lattice artifacts could be significant. This consistency corroborates the universality of the lattice-determined CS kernel and suggests that a high-precision determination of it is in reach.

Introduction. The description of the internal structure of hadrons is a fundamental problem of QCD. The present description of high-energy processes is founded on factorization theorems, which express the cross-sections of reactions in terms of calculable perturbative parts and universal nonperturbative functions, also known as parton distributions. In the modern era, the emphasis of studies is shifting towards multi-dimensional observables [1, 2] and multi-dimensional parton distributions, such as transverse momentum dependent parton distribution functions (TMDPDFs) [3]. TMDPDFs encode the information about the 3D parton momenta inside a hadron. TMDPDFs are universal, in the sense that they are dependent on the types of parton and hadron but not on the processes. This universality is the cornerstone of the factorization approach. In the case of TMDPDFs, it has been indirectly confirmed by many phenomenological extractions, which utilize multiple processes [4–11].

The evolution of TMDPDFs over the rapidity scale ζ can be described by

$$2\zeta \frac{d}{d\zeta} \ln \Phi_{f/h}(x, b, \mu, \zeta) = K(b, \mu), \quad (1)$$

which also provides the simplest way to access the CS kernel $K(b, \mu)$ —the topic of this study. $\Phi_{f/h}$ is a TMDPDF of flavor f in hadron h with x being the longitudinal momentum fraction, and b being the transverse distance, at scale μ . The evolution equation holds for TMDPDFs of any kind, including also twist-3 TMDPDFs, as was derived recently [12–14]. The CS kernel is one of the most fundamental nonperturbative functions in QCD since it describes the interaction of a parton with the QCD vacuum [15] and appears in the description of many types of processes, including inclusive ones

[16], exclusive ones [17], and jet-production [18]. Being a vacuum-determined function, the CS kernel obeys a stronger universality – it is independent of any quantum numbers except the color representation of the probe (quark or gluon). The confirmation of this universality for the CS-kernel is of fundamental importance for QCD.

Traditionally, the CS kernel is determined from fits of scattering data, along with TMDPDFs; see [7, 8, 19] for examples. However, this approach requires assumption of a functional form and, thus, is biased. Recently a number of more direct ways were proposed. All these methods suggest to determine the CS kernel from the ratio of properly constructed observables – cross-sections [20] or quasi-TMDPDFs [21–23]. The latter can be achieved by lattice QCD simulations, which have been done in Refs. [21, 24–27]. The lattice determination of CS kernel demonstrated high potency, especially for large- b values that can not be accessed in collider experiments. So far, all simulations are done for unpolarized quasi-TMDPDFs of the proton. The only exception is [25], where also polarized quasi-TMDPDFs are used.

In this Letter, we present a new set of lattice computations of the CS kernel. For the first time, we use four principally different setups. Namely, we use proton and pion targets, and twist-two and twist-three quasi-TMDPDF operators. Comparing these cases provides confirmation of the universality of the CS kernel and further constrains its form.

Theoretical framework. We consider the following matrix element (quasi-TMDPDF)

$$W_{f/h}^{[\Gamma]}(b; \ell, L; v, P, S; \mu) = \langle h(P, S) | \bar{q}_f(b + \ell v) \Gamma \mathcal{U}[\mathcal{C}(\ell, v, b, L)] q_f(0) | h(P, S) \rangle, \quad (2)$$

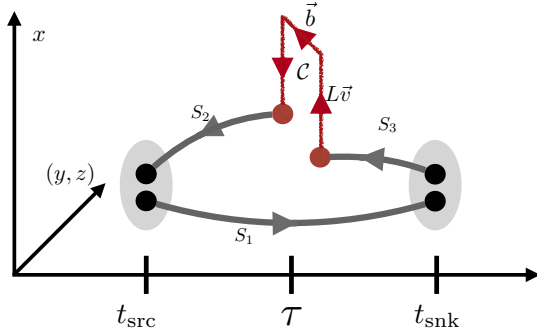


FIG. 1. Illustration of the pion matrix element, see Eq.(2). The two external pion states are shown as grey ovals. The non-local quark current is shown in red, made up of a quark-antiquark pair (the red points) connected by a staple-shaped gauge link C . The matrix element is calculated on the lattice using the sequential source method. The sequential source is constructed using propagators S_1 and S_3 . For the proton an additional direct propagator from source to sink is needed.

where $|h(P, S)\rangle$ is a single-hadron state with momentum P and spin S . Γ is a Dirac matrix and f indicates the flavor of the quark-field. The staple-shaped Wilson link \mathcal{U} is of length L stretching in the direction $v^\mu = (0, \pm 1, 0, 0)$ and of width \vec{b} pointing in a transverse spatial direction. Note that the quark-antiquark pair connected by the Wilson link is positioned in the same imaginary time slice. The offset distance of the quark-antiquark pair along v is denoted by ℓ . The structure of the matrix element is visualized in the sketch in Fig. 1.

At large L and hadron momentum, the matrix element (2) can be factorized [21–23, 28, 29]. The structure of the factorization theorem crucially depends on Γ . In particular, for $\Gamma = \{\gamma^0, \gamma^5, \dots\}$ (the complete set can be found in Ref. [30]) one has the so-called leading power (LP) expression

$$W_{f/h}^{[\Gamma]}(x; b; P; \mu) = \left(\frac{2|x|(P^+)^2}{\zeta} \right)^{K(b, \mu)/2} \times \mathbb{C}_H(xP^+, \mu) \Phi_{f/h}^{[\Gamma]}(x, b; \mu, \zeta) + \mathcal{O}(\lambda^2), \quad (3)$$

where $P^+ = (E_P + P_x)/\sqrt{2}$, $P^\mu = (E_P, P_x, 0, 0)$, and Φ is the physical TMDPDF and \mathbb{C}_H is the coefficient function. The coefficient functions \mathbb{C}_H are known at next-to-leading order (NLO) in the QCD coupling constant [21–23]. The variable x is the momentum fraction, Fourier-conjugate to ℓP_x . The correction term $\mathcal{O}(\lambda^2)$ contains various power-suppressed terms

$$\mathcal{O}(\lambda^2) = \mathcal{O}\left(\frac{M^2}{(xP^+)^2}, \frac{1}{(bP^+)^2}, \frac{b}{L}, \frac{1}{ML}\right), \quad (4)$$

with M being the mass of the hadron.

The left hand side of Eq. (3) is independent of the parameter ζ . Thus, the ratio of quasi-TMDPDFs at the same parameters except for momenta eliminates the

hadronic component of the factorization theorem,

$$R^{[\Gamma]}(x, b, \mu; P_1, P_2) = \frac{W_{f/h}^{[\Gamma]}(x, b; P_1, S; \mu)}{W_{f/h}^{[\Gamma]}(x, b; P_2, S; \mu)} = \left(\frac{P_1^+}{P_2^+} \right)^{K(b, \mu)} \frac{\mathbb{C}_H(xP_1^+, \mu)}{\mathbb{C}_H(xP_2^+, \mu)} + \mathcal{O}(\lambda^2). \quad (5)$$

Inverting this relation one determines the CS-kernel.

One should note that for this way to proceed, a Fourier transformation of the quasi-TMDPDF from coordinate space (ℓP_x) to momentum-fraction space (x) is required. Such a transformation has to be supplemented by model assumptions concerning the tail of the quasi-TMDPDF [27], which introduces additional systematic uncertainty. A procedure which avoids this complication was proposed in Ref. [23]. It is suggested to analyse the ratio of the first Mellin moments ($\ell = 0$) of two quasi-TMDPDFs. In this case, the ratio can be written as

$$R^{[\Gamma]}(P_1, P_2; b) = \left(\frac{P_1^+}{P_2^+} \right)^{K(b, \mu)} \mathbf{r}^{[\Gamma]}(b, \mu; P_1, P_2), \quad (6)$$

where \mathbf{r} is [23]

$$\mathbf{r}^{[\Gamma]}(b, \mu; P_1, P_2) = 1 + 4C_F \frac{\alpha_s(\mu)}{4\pi} \ln \left(\frac{P_1^+}{P_2^+} \right) \times \left[1 - \ln \left(\frac{2P_1^+ P_2^+}{\mu^2} \right) - 2\mathbf{M}^{[\Gamma]}(b, \mu) \right]. \quad (7)$$

The function \mathbf{M} contains the residual terms of the perturbative expansion, and depends on the quantum numbers of the quasi-TMDPDF. A key argument underlying this method is that the function $\mathbf{M}^{[\Gamma]}(b, \mu)$ is almost independent of b . This assumption is based on the weak correlation of b and x dependencies of TMDPDFs, which has been verified by fitting experimental data with the unpolarized TMDPDFs for the proton and pion [6, 7]. The value of \mathbf{M} can be found by comparing Eq. (7) and its value in perturbation theory at $b \sim 1 \text{ GeV}^{-1}$ and $\mu_0 = 2 \text{ GeV}$ (where both perturbation theory and the factorization theorem are valid). For extended details see Ref. [25]. The method is much simpler in comparison to Eq. (5) but cannot be improved beyond NLO.

The description of the cases $\Gamma = \{\mathbb{1}, \gamma^5, \dots\}$ requires the next-to-leading power (NLP) factorization theorem [30]. The NLP factorization has a much more involved form and expresses a single quasi-TMDPDF via a sum of various physical TMDPDFs, and also new lattice-related nonperturbative functions $\Psi_{21}(b)$ and $\Psi_{12}(b)$ [30]. The complicated structure of NLP factorization makes it less practical. However, for particular combinations of Γ and polarization, the NLP factorization simplifies to the form of Eq. (3) (with a different coefficient function). In these cases, one can use the method Eq. (6) to determine the CS-kernel (note, however, that considering the ratios

TABLE I. Lattice setup used in this study.

Ensemble	a [fm]	$N_\sigma^3 \times N_\tau$	m_π^{sea}	#conf
H101	0.0854	$32^3 \times 96$	422 MeV	2016

Eq. (5) is not helpful due to the x -dependence of \mathbb{C}_H at NLP). The simple cases include $\Gamma = \mathbb{1}$ for the TMDPDF $e(x, b)$.

Lattice calculation. The matrix element Eq. (2) can be calculated as the ratio of a three-point and a two-point function on the lattice,

$$W^{[\Gamma]} = 2E_P \lim_{0 \ll \tau \ll t} \frac{C_{3pt}(P, \mathcal{C}, t, \tau, \Gamma)}{C_{2pt}(P, t)}, \quad (8)$$

where E_P is the energy of the hadron extracted from the two-point function. In the continuum limit, the lattice definition Eq. (8) reproduces the continuum definition, see e.g. Ref. [31]. The parameters t and τ are the source-sink separation and the temporal distance between the source and the inserted non-local quark current. The three-point function is defined as

$$C_{3pt}^\Gamma(\vec{P}, \mathcal{C}, t, \tau, \Gamma) \equiv \left\langle \text{tr} \left\{ \Gamma_S \mathcal{O}(\vec{P}, t) J^\Gamma(\mathcal{C}, \tau) \overline{\mathcal{O}}(\vec{P}, 0) \right\} \right\rangle \quad (9)$$

and calculated using the sequential source method [32] with hadron interpolator $\mathcal{O}(\vec{P}, t)$. The non-local quark current reads

$$J^\Gamma(\mathcal{C}, \tau) \equiv \bar{q}(b, \tau) \Gamma \mathcal{U}[\mathcal{C}(v, b, L)] q(0, \tau), \quad (10)$$

where q can be either up quark or down quark, and $\mathcal{U}[\mathcal{C}(v, b, L)]$ is the staple-shaped Wilson link, as illustrated in Fig.1. The two-point function is

$$C_{2pt}(\vec{P}, t) \equiv \left\langle \text{tr} \left\{ \Gamma_S \mathcal{O}(\vec{P}, t) \overline{\mathcal{O}}(\vec{P}, 0) \right\} \right\rangle, \quad (11)$$

where $\Gamma_S = (1 + \gamma_4)(1 - i\gamma_2\gamma_1)/2$ is needed for the proton to project out the desired parity and spin. For the pion Γ_S is not necessary and is set to unity. In the calculation of the matrix element, we have adopted HYP smearing for the gauge links [33] and the momentum smearing technique [34] to improve the signal. We analyse the CLS ensemble H101 generated using $N_f = 2 + 1$ flavors of clover-improved Wilson fermions [35]. The lattice setup is summarized in Tab.I.

The analysis for the proton re-uses the data generated in [25], where the source-sink separation is $t_{\text{sink}} - t_{\text{src}} = 11a$ and the valence quark is the same as the sea quark. In the pion case, the simulation with the same setup appears much noisier. To reduce the noise, we use a heavier valence quark corresponding to $m_\pi^{val} = 686$ MeV. We do not expect a substantial mass dependence of the resulting CS kernel. In the physical limit, at large boost factors, the CS kernel depends weakly on the quark mass, see,

e.g., Ref. [26]. Besides, we use a smaller source-sink separation (9a) to further increase the signal for the three- and two-point functions.

In the analysis of the pion data, we have fitted the ratio to a constant in the interval $\tau \in [4a, 6a]$, where the excited states are suppressed. The simulation has been done for six momenta $P_1 \in \{0, 1, 2, 3, 4, 5\} \frac{2\pi}{aN_\sigma}$, but only the first three nonzero momenta have sufficient signal/noise ratio to be processed further. We have confirmed that the extracted energies respect the dispersion relation $E_P = \sqrt{M^2 + P_1^2}$ within statistical errors. We have also confirmed that our results respect the charge conservation condition $C_{3pt}(t, \tau, \gamma^0)/C_{2pt}(t) = 1/Z_V$, where Z_V is the renormalization constant for the quark field in the vector channel [36] and $C_{3pt}(t, \tau, \gamma^0)$ is the local three-point function. For non-local correlations, we considered transverse separations in the y - or z -direction (or a combination of both), with lengths $\{1, \sqrt{2}, 2, \dots, 8, 6\sqrt{2}, 9\}a$. The size of the staple-link L was taken as large as possible to fulfill the condition Eq. (4) on the premise that the signal for the three-point function is acceptable.

As detailed in Refs. [31, 37–39], the hadron matrix elements Eq. (8) in different channels (with different Γ matrix insertion) can be parameterized using invariant amplitudes \tilde{A}_i and \tilde{B}_i . In the case of the pion the parameterization is [38]

$$\begin{aligned} W^{[\gamma^0]} &= E_P \tilde{A}_2, \\ W^{[\gamma^1]} &= P_x \tilde{A}_2 + M^2 \frac{v^{[1]}}{(v \cdot P)} \tilde{B}_1, \\ W^{[\mathbb{1}]} &= M \tilde{A}_1. \end{aligned} \quad (12)$$

Thus the relevant amplitudes can be obtained from a combination of matrix elements in the three channels γ_0 , γ_1 and $\mathbb{1}$. Combining the available amplitudes from the decomposition, we obtain the quasi-TMDPDFs

$$\begin{aligned} f_1(b^2, P^+) &= P^+ (\tilde{A}_2(b^2) + M^2 \frac{v^+}{(v \cdot P) P^+} \tilde{B}_1(b^2)), \\ e(b^2, P^+) &= P^+ \tilde{A}_1(b^2), \end{aligned} \quad (13)$$

which satisfy the LP (f_1) and NLP (e) factorization theorem [30].

Numerical results: The pair of momenta used, $P_x = \{2, 3\} \times \frac{2\pi}{aN_\sigma}$ for both pion and proton, corresponds to $P^-/P^+ = \{0.13, 0.07\}$ for the pion and $P^-/P^+ = \{0.25, 0.14\}$ for the proton, such that $M^2/(xP^+)^2$ is not large in Eq. (4). We also analysed the pair of momenta $P_x = \{1, 2\} \times \frac{2\pi}{aN_\sigma}$ for the pion. This case has larger systematic biases from the power corrections in Eq. (4) that we cannot reliably quantify; on the other hand, the pair of larger momenta has larger statistical uncertainties. We do not know for which combination the total uncertainty is larger. We present our final results in Fig. 3 for $P_1/P_2 = 3/2$, i.e., with the larger statistical errors,

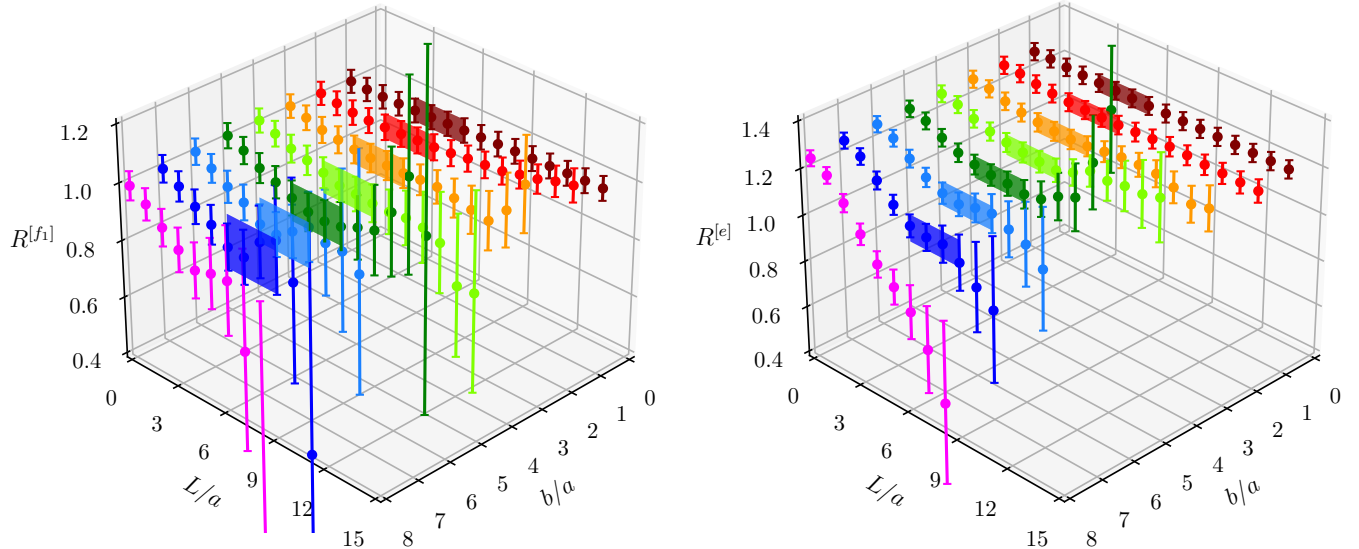


FIG. 2. Lattice results for the ratios $R^{[f_1]}$ and $R^{[e]}$ in the pion case from the momentum pair $\{P_1^+, P_2^+\} = \{2.07, 1.48\}$ GeV at different transverse separations b . The colored bands indicate the results of constant fits in the L -interval $[4a, 7a]$.

and give the analog for $P_1/P_2 = 2/1$ in the Supplementary Material. $1/(bP^+)^2 \ll 1$ for Eq. (4) is fulfilled if $b \gg \{1.8a, 1.1a\}$, implying that our extracted CS kernel is valid at $b > 0.15$ fm. Finally, to make b/L and $1/(ML)$ small, L should be taken as large as possible. For large L the ratio should saturate and show a plateau. We have found that this happens in the interval $[4a, 7a]$ for both f_1 and e at all values of b for the pion, see Fig. 2. Similar figures for the proton are presented in the Supplementary Material. Still larger values of L can also be included into the fit with, however, negligible impact on the fit's quality. To increase the statistics and reduce systematic uncertainties, we have combined the data with L stretching in the positive and negative v directions. Both directions should be equivalent as a consequence of parity symmetry.

The value of the constant \mathbf{M} is determined following the procedure described in Ref. [25]. We use a reference transverse separation $b_0 = 3a = 0.26$ fm = 1.3 GeV $^{-1}$, for which the value of the CS kernel is safely known from perturbative computations [40–42] and from phenomenological extractions [7, 9] (all agree with each other up to small corrections). At the same time, the terms in Eq. (4) are small. We normalize the value of the CS kernel at this point (explicitly, we use the values of the phenomenological extraction SV19 [7] at N³LO). Our estimate for \mathbf{M} is $-0.83(0.73)$ for f_1 (pion), $-4.98(0.61)$ for e (pion), $-0.57(0.34)$ for f_1 (proton), and $-1.04(1.32)$ for e (proton). The uncertainty in the estimation of \mathbf{M} results in a fully correlated uncertainty for the CS kernel δK . The values of δK are $\{0.15, 0.10, 0.08, 0.27\}$ for f_1 (pion), e (pion), f_1 (proton) and e (proton), correspondingly. Nevertheless,

δK is not shown in Figs. 3 and figures in the Supplementary Material as it is correlated with the statistical uncertainty and cannot be simply added as an independent uncertainty.

The resulting values of the CS kernel are plotted in Fig. 3. Note that the error bars shown in Fig. 3 are purely statistical. In the left panel of Fig. 3, the data points with $b > 7a$ are plotted with light colors and grey error bars to indicate that the extracted values suffer from uncontrolled systematic uncertainties. In this region, plateaus of R are not reached even for maximal values of L , as can be seen from Fig. 2. Additionally, the points at small $b < 0.8$ GeV $^{-1}$ are contaminated by power corrections $\sim b^{-2}$. Therefore, our main results are the points in the intermediate region.

In the left panel of Fig. 3, we compare our results with those of a 3-loop perturbative calculation [41] and two phenomenological extractions, SV19 [7] and MAP22 [9]. We observe good agreement with the SV19 fit, while MAP22 has smaller absolute values. In the right panel of Fig. 3, we compare our results with other lattice computations [24, 26, 27, 43, 44]. The first three [24, 26, 27] were calculated from quasi-TMDWFs in full QCD, while the Hermite and Bernstein results [43] are from quasi-TMDPDFs in the quenched approximation. The points obtained in Ref. [44] are roughly an extension of the former quenched results [43] to full QCD. All lattice computations display qualitatively similar behavior. The discrepancies among them can be understood as systematic effects, since most calculations differ in important aspects. For example, the computation [27] is based on 1-loop matching while the computation in [24] is based

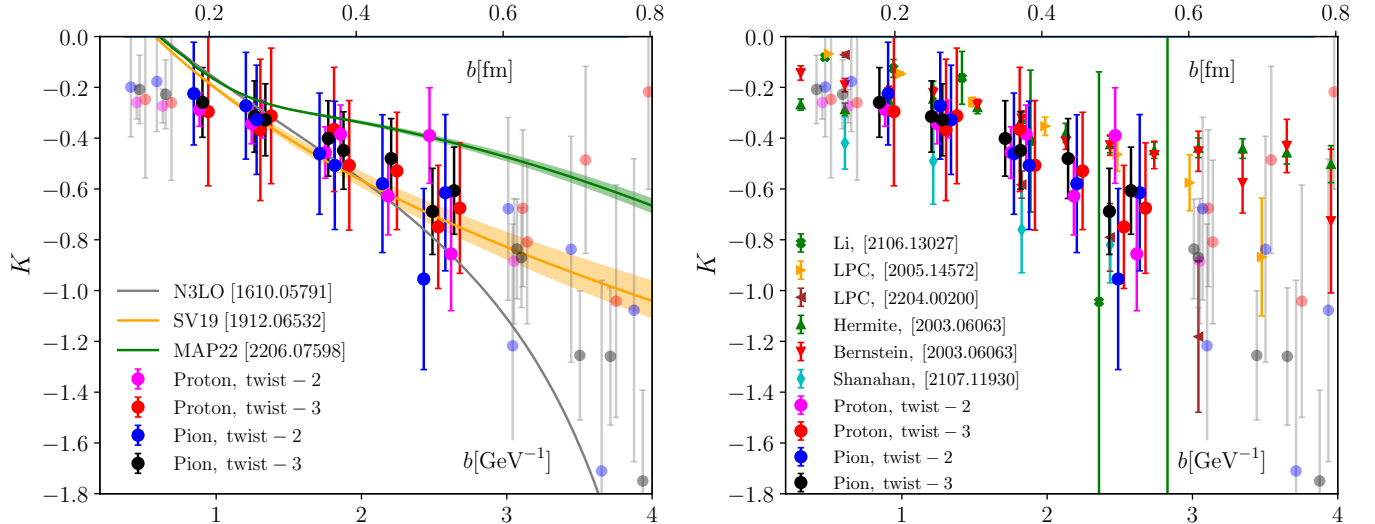


FIG. 3. Comparison of CS kernel obtained in this work to those from other studies. *Left*: comparison to the 3-loop perturbative calculation [41] and two phenomenological extractions, SV19 [7] and MAP22 [9]. *Right*: Comparison with other lattice studies [24, 26, 27, 43] based on LaMET. The points are slightly shifted horizontally for better visibility in both panels.

on tree-level matching.

We remark that pion states possess higher symmetry, which precludes some systematic contaminations stemming, e.g., from the lattice discretization that may additionally affect the proton state. Formally, this is reflected in the fact that fewer amplitudes are involved in the parametrization for the pion, leading to more constrained systematic uncertainties when solving for the amplitudes. In this regard, our computations with pion states are more reliable. The most important observation is that all four of our computations agree with each other where they are reliable. This confirms the universality of the CS kernel with respect to the particle type. The agreement between the extractions based on f_1 and e distributions confirms the validity of Eq. (1) for twist-3 TMDPDFs, which was derived in Refs. [12–14].

Conclusion: We have extracted the Collins-Soper kernel from the first Mellin moment of pion and proton quasi-TMDPDFs on the CLS ensemble H101. To improve the signal-to-noise ratio, we applied HYP smearing and momentum smearing. To extract the CS kernel we used the approach proposed in Ref. [23] based on NLO factorization of the quasi-TMDPDF. We obtained reliable results in the range $0.8 \text{ GeV}^{-1} \lesssim b \lesssim 2.6 \text{ GeV}^{-1}$. In this range, our results agree well with the phenomenological extraction SV19 [7], the lattice calculation [44], and another one [27] based on 1-loop matching in the LaMET framework. The extrapolation of all results to physical masses and the continuum is not yet well under control. The main challenge for future work is to investigate and quantify all sources of systematic uncertainties.

The key feature of this extraction is that we used four independent matrix elements to determine the CS ker-

nel, namely, the unpolarized quasi-TMDPDF f_1 and the quasi-TMDPDF e with proton and pion states. The quasi-TMDPDFs f_1 and e obey different kinds of factorization theorems – in leading and next-to-leading power, correspondingly. The agreement between these extractions provides a strong check of the universality of the CS kernel. It is the first direct confirmation of this property. Also, for the first time, our work checks the predictions of NLP factorization theory [30], and confirms them.

ACKNOWLEDGMENTS

We acknowledge PRACE for awarding us access to SuperMUC-NG at GCS@LRZ, Germany. The authors thank the Rechenzentrum of Regensburg for providing the Athene Cluster for supplementary computations. We thank the CLS Collaboration for sharing the lattices used to perform this study. The LQCD calculations were performed using the multigrid algorithm [45, 46] and Chroma software suite [47]. We also thank Gunnar Bali, Sara Collins and Christian Zimmermann for helpful discussions. HTS, AS, MS, LW and YY are supported by a NSFC-DFG joint grant under grant No. 12061131006 and SCHA 458/22. YY is also supported in part by the Strategic Priority Research Program of Chinese Academy of Sciences, Grant No. XDB34030300 and XDPB15, and also by the National Natural Science Foundation of China (NSFC) under Grants No. 12293062. AV is funded by the *Atracción de Talento Investigador* program of the Comunidad de Madrid (Spain) No. 2020-T1/TIC-20204. AV is also supported by the Spanish Ministry grant PID2019-106080GB-C21. ME is supported by the

U.S. Department of Energy, Office of Science, Office of Nuclear Physics through grant DE-FG02-96ER40965 and through the TMD Topical Collaboration.

[1] S. Amoroso *et al.*, (2022), arXiv:2203.13923 [hep-ph].

[2] R. Abdul Khalek *et al.*, (2022), arXiv:2203.13199 [hep-ph].

[3] R. Angeles-Martinez *et al.*, *Acta Phys. Polon. B* **46**, 2501 (2015), arXiv:1507.05267 [hep-ph].

[4] I. Scimemi and A. Vladimirov, *Eur. Phys. J. C* **78**, 89 (2018), arXiv:1706.01473 [hep-ph].

[5] V. Bertone, I. Scimemi, and A. Vladimirov, *JHEP* **06**, 028 (2019), arXiv:1902.08474 [hep-ph].

[6] A. Vladimirov, *JHEP* **10**, 090 (2019), arXiv:1907.10356 [hep-ph].

[7] I. Scimemi and A. Vladimirov, *JHEP* **06**, 137 (2020), arXiv:1912.06532 [hep-ph].

[8] A. Bacchetta, V. Bertone, C. Bissolotti, G. Bozzi, F. Delcarro, F. Piacenza, and M. Radici, *JHEP* **07**, 117 (2020), arXiv:1912.07550 [hep-ph].

[9] A. Bacchetta, V. Bertone, C. Bissolotti, G. Bozzi, M. Cerutti, F. Piacenza, M. Radici, and A. Signori (MAP), *JHEP* **10**, 127 (2022), arXiv:2206.07598 [hep-ph].

[10] M. Bury, A. Prokudin, and A. Vladimirov, *Phys. Rev. Lett.* **126**, 112002 (2021), arXiv:2012.05135 [hep-ph].

[11] M. G. Echevarria, Z.-B. Kang, and J. Terry, *JHEP* **01**, 126 (2021), arXiv:2009.10710 [hep-ph].

[12] A. Vladimirov, V. Moos, and I. Scimemi, *JHEP* **01**, 110 (2022), arXiv:2109.09771 [hep-ph].

[13] M. A. Ebert, A. Gao, and I. W. Stewart, *JHEP* **06**, 007 (2022), arXiv:2112.07680 [hep-ph].

[14] S. Rodini and A. Vladimirov, *JHEP* **08**, 031 (2022), [Erratum: *JHEP* 12, 048 (2022)], arXiv:2204.03856 [hep-ph].

[15] A. A. Vladimirov, *Phys. Rev. Lett.* **125**, 192002 (2020), arXiv:2003.02288 [hep-ph].

[16] J. Collins, *Foundations of perturbative QCD*, Vol. 32 (Cambridge University Press, 2013).

[17] M. G. Echevarria, P. A. Gutierrez Garcia, and I. Scimemi, (2022), arXiv:2208.00021 [hep-ph].

[18] D. Neill, I. Scimemi, and W. J. Waalewijn, *JHEP* **04**, 020 (2017), arXiv:1612.04817 [hep-ph].

[19] F. Landry, R. Brock, G. Ladinsky, and C. P. Yuan, *Phys. Rev. D* **63**, 013004 (2001), arXiv:hep-ph/9905391.

[20] A. Bermudez Martinez and A. Vladimirov, *Phys. Rev. D* **106**, L091501 (2022), arXiv:2206.01105 [hep-ph].

[21] M. A. Ebert, I. W. Stewart, and Y. Zhao, *Phys. Rev. D* **99**, 034505 (2019), arXiv:1811.00026 [hep-ph].

[22] X. Ji, Y. Liu, and Y.-S. Liu, *Nucl. Phys. B* **955**, 115054 (2020), arXiv:1910.11415 [hep-ph].

[23] A. A. Vladimirov and A. Schäfer, *Phys. Rev. D* **101**, 074517 (2020), arXiv:2002.07527 [hep-ph].

[24] Q.-A. Zhang *et al.* (LPC), *Phys. Rev. Lett.* **125**, 192001 (2020), arXiv:2005.14572 [hep-lat].

[25] M. Schlemmer, A. Vladimirov, C. Zimmermann, M. Engelhardt, and A. Schäfer, *JHEP* **08**, 004 (2021), arXiv:2103.16991 [hep-lat].

[26] Y. Li *et al.*, *Phys. Rev. Lett.* **128**, 062002 (2022), arXiv:2106.13027 [hep-lat].

[27] M.-H. Chu *et al.* (LPC), *Phys. Rev. D* **106**, 034509 (2022), arXiv:2204.00200 [hep-lat].

[28] X. Ji and Y. Liu, *Phys. Rev. D* **105**, 076014 (2022), arXiv:2106.05310 [hep-ph].

[29] M. A. Ebert, S. T. Schindler, I. W. Stewart, and Y. Zhao, *JHEP* **04**, 178 (2022), arXiv:2201.08401 [hep-ph].

[30] S. Rodini and A. Vladimirov, (2022), arXiv:2211.04494 [hep-ph].

[31] B. U. Musch, P. Hägler, J. W. Negele, and A. Schäfer, *Phys. Rev. D* **83**, 094507 (2011), arXiv:1011.1213 [hep-lat].

[32] G. Martinelli and C. T. Sachrajda, *Nucl. Phys. B* **316**, 355 (1989).

[33] A. Hasenfratz and F. Knechtli, *Phys. Rev. D* **64**, 034504 (2001), arXiv:hep-lat/0103029.

[34] G. S. Bali, B. Lang, B. U. Musch, and A. Schäfer, *Phys. Rev. D* **93**, 094515 (2016), arXiv:1602.05525 [hep-lat].

[35] M. Bruno *et al.*, *JHEP* **02**, 043 (2015), arXiv:1411.3982 [hep-lat].

[36] G. S. Bali, S. Bürger, S. Collins, M. Göckeler, M. Gruber, S. Piemonte, A. Schäfer, A. Sternbeck, and P. Wein, *Phys. Rev. D* **103**, 094511 (2021), arXiv:2012.06284 [hep-lat].

[37] B. Musch, P. Hägler, M. Engelhardt, J. Negele, and A. Schäfer, *Phys. Rev. D* **85**, 094510 (2012), arXiv:1111.4249 [hep-lat].

[38] M. Engelhardt, P. Hägler, B. Musch, J. Negele, and A. Schäfer, *Phys. Rev. D* **93**, 054501 (2016), arXiv:1506.07826 [hep-lat].

[39] B. Yoon, M. Engelhardt, R. Gupta, T. Bhattacharya, J. R. Green, B. U. Musch, J. W. Negele, A. V. Pochinsky, A. Schäfer, and S. N. Syritsyn, *Phys. Rev. D* **96**, 094508 (2017), arXiv:1706.03406 [hep-lat].

[40] M. G. Echevarria, A. Idilbi, A. Schäfer, and I. Scimemi, *Eur. Phys. J. C* **73**, 2636 (2013), arXiv:1208.1281 [hep-ph].

[41] A. A. Vladimirov, *Phys. Rev. Lett.* **118**, 062001 (2017), arXiv:1610.05791 [hep-ph].

[42] I. Moult, H. X. Zhu, and Y. J. Zhu, *JHEP* **08**, 280 (2022), arXiv:2205.02249 [hep-ph].

[43] P. Shanahan, M. Wagman, and Y. Zhao, *Phys. Rev. D* **102**, 014511 (2020), arXiv:2003.06063 [hep-lat].

[44] P. Shanahan, M. Wagman, and Y. Zhao, *Phys. Rev. D* **104**, 114502 (2021), arXiv:2107.11930 [hep-lat].

[45] R. Babich, J. Brannick, R. C. Brower, M. A. Clark, T. A. Manteuffel, S. F. McCormick, J. C. Osborn, and C. Rebbi, *Phys. Rev. Lett.* **105**, 201602 (2010), arXiv:1005.3043 [hep-lat].

[46] J. C. Osborn, R. Babich, J. Brannick, R. C. Brower, M. A. Clark, S. D. Cohen, and C. Rebbi, *Proceedings, 28th International Symposium on Lattice field theory (Lattice 2010): Villasimius, Italy, June 14-19, 2010, PoS LATTICE2010*, 037 (2010), arXiv:1011.2775 [hep-lat].

[47] R. G. Edwards and B. Joo (SciDAC, LHPC, UKQCD), *Lattice field theory. Proceedings, 22nd International Symposium, Lattice 2004, Batavia, USA, June 21-26, 2004, Nucl. Phys. Proc. Suppl.* **140**, 832 (2005), arXiv:hep-lat/0409003 [hep-lat].

SUPPLEMENTAL MATERIALS

In this supplemental material we first show the constant fit of the ratio R in L for proton in Fig. 4. It can be seen the change pattern is similar as in the pion case but the fit interval needs to be adjusted accordingly.

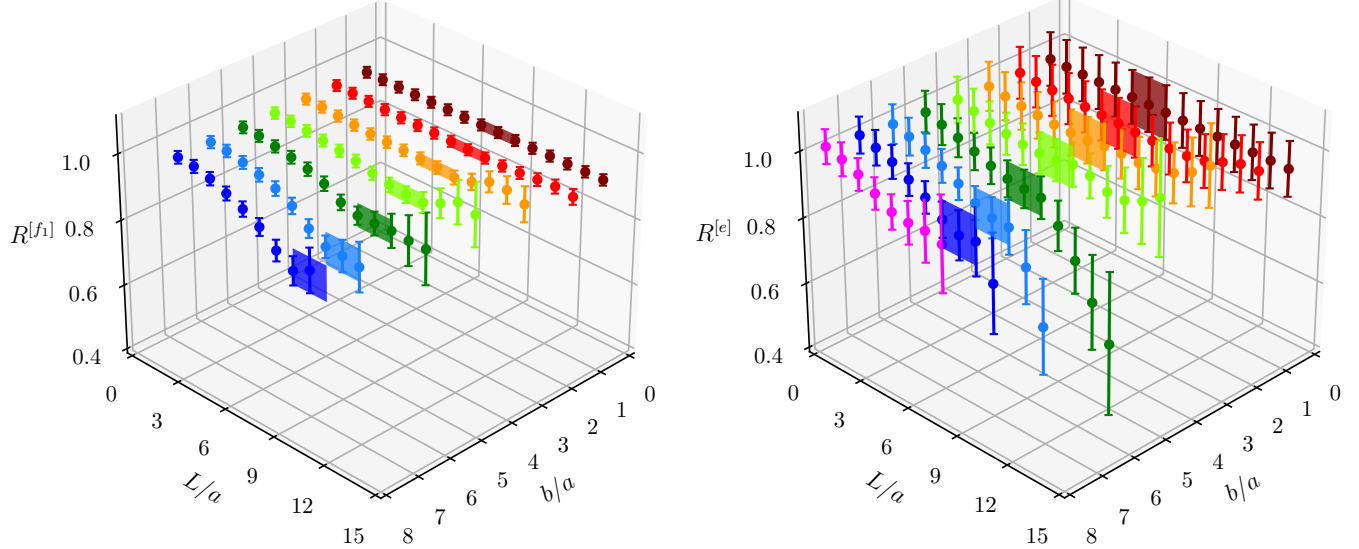


FIG. 4. Lattice results for the ratios $R^{[f_1]}$ and $R^{[e]}$ in the proton case from the momentum pair $P_1/P_2 = 3/2$ at different transverse separations b . The colored bands indicate the results of constant fits in the L -interval $[8a, 10a]$ for f_1 and $[6a, 8a]$ for e .

Then we present the results for the CS kernel extracted from the momentum pair $P_1/P_2 = 2/1$ in the pion case. The ratio of the matrix elements for f_1 and e are shown in Fig. 5. Compared to the larger momentum case the plateau appears at larger L for small momentum. We fit the ratio to a constant in the intervals $[6a, 9a]$ for f_1 and $[8a, 11a]$ for e at all values of b . The plateaus can be identified with much smaller statistical uncertainties, as expected.

We compare the extracted CS kernel from different momentum pairs in Fig. 6. Consistent values for the CS kernel can be observed for all b for which the data is reliable. This indicates that the power corrections may be strongly suppressed even at the smallest momentum considered in this work. In addition, the insensitivity of the CS kernel to $M^2/(xP^+)^2$ also supports the rationale of using a large valence quark mass in our calculation *a posteriori*.

|

